Article:
Wang, J.Y, Healey, T., Barker, A. et al. (2017) Magnetic induction spectroscopy (MIS)—probe design for cervical tissue measurements. Physiological Measurement, 38 (5). pp. 729-744. ISSN: 0967-3334

https://doi.org/10.1088/1361-6579/aa6b4e

Magnetic Induction Spectroscopy (MIS) - Probe Design for Cervical Tissue Measurements

Jau-Yi Wang[1], Timothy Healey[2], Anthony Barker[2], Brian Brown[3], Chris Monk[2], Dilly Anumba[1]

[1] Academic Unit of Reproductive and Development Medicine, Jessop Wing, University of Sheffield and Sheffield Teaching Hospitals NHS Trust, Sheffield S10 2SF, UK
[2] Medical Physics and Clinical Engineering, University of Sheffield and Sheffield Teaching Hospital NHS Trust, Glossop Road, Sheffield S10 2JF, UK
[3] Department of Medical Physics and Engineering, University of Sheffield, Beech Hill Road, Sheffield S10 2RX, UK

E-mail: d.o.c.anumba@sheffield.ac.uk

Abstract

Gradiometers have the advantage of increasing measuring sensitivity, which is particularly useful in magnetic induction spectroscopy (MIS) for bio-impedance measurements. Traditional gradiometers use a pair of field sensing coils equally distant and on opposite sides of a drive coil, which provides high immunity to interference. In this paper, a ferrite-cored coaxial gradiometer probe of 29 mm diameter has been developed for measuring the impedance spectra of cervical tissues in vivo. It consists of a ferrite rod with outer ferrite confinement screening in order to eliminate the signals from surrounding tissue. The magnetic screening efficiency was compared with an air-cored gradiometer probe. For both gradiometer probes, a drive coil and two sensing coils were wound on a borosilicate glass former aligned coaxially with two sensing coils equidistant from the drive coil. The signal sensitivity of those two MIS gradiometers has been measured using saline samples with a conductivity range between 0.1 and 1.1 Sm^{-1}. Finite element methods using COMSOL Multiphysics have been used to simulate the distribution of sensitivity to conductivity over the face of each probe and with depth. The ferrite-cored probe has a sensitivity confined to the volume defined by the gap between the ferrite core and outer tube of ferrite while the air-cored probe without any magnetic shielding had a wide sensitivity over the face and the side of the probe. Four saline samples and one of distilled water with conductivities from 0.1 to 1.1 Sm^{-1} have been used to make conductivity measurements at frequencies of 50 kHz, 100 kHz, and 300 kHz. The measurement accuracy of the air-cored MIS probe was 0.09 Sm^{-1} at 50 kHz, improving to 0.05 Sm^{-1} at 300 kHz. For the ferrite-cored MIS probe, the measurement accuracy was 0.28 Sm^{-1} at 50 kHz, improving to 0.04 Sm^{-1} at 300 kHz.

Keywords: magnetic induction spectroscopy, gradiometer, tissue impedance

1. Introduction

1.1 Physiological background

The electrical properties of biological tissues have been studied for over a century. When measuring over a frequency range from dc to a few GHz, the electrical permittivity and conductivity of biological tissues have been found to be dependent on frequency (Gabriel *et al* 1996a, Gabriel *et al* 1996b, Krazewski *et al* 1982, McAdams and Jossinet 1995, Schwan and Kay 1957). These electrical parameters are determined by the cellular structure and arrangement in addition to the binding of the ions within the tissue components (Schwan and Foster 1980). In general, three main distinct regions called dispersions have been found in the dielectric spectra, which are referred to as the α, β, and γ dispersions (Miklavcic *et* al 2006, Schwan 1994). The α dispersion mainly occurs between dc and a few hundred hertz and is related to the larger structures such as membranes and sheets of cells. The β dispersion occurs between a few kHz and about 10 MHz and is determined by cell arrangements and current flow across cellular membranes. The γ dispersion mainly occurs in the gigahertz region and is related to the dielectric relaxation of molecules (Foster and Schwan 1995, Schwan 1994). For biological tissues, dielectric measurements of the β dispersion have been found to

be particularly useful, due to the sensitivity to tissue structures and the relative sizes of the intracellular and extracellular fluid volumes (Foster and Schwan 1995, Schwan and Foster 1980, Stoy *et al* 1982).

Traditionally, dielectric measurements on biological tissues in the β dispersion range have been made by making contact with the tissues using two, three or four electrodes (Burger and van Dongen 1960, Hart and Dunfee 1993, Martinsen and Grimnes 2011, Yamamoto and Yamamoto 1987). The technique is usually referred to as electrical impedance spectroscopy (EIS) (Abdul *et al* 2006, Aberg *et al* 2004, Dean 2008, Gandhi *et al* 2006, Gersing 1998, Halter *et al* 2007, Kerner *et al* 2002, Osterman 2004). The contact between sample and electrodes causes one of the main challenges in EIS measurements (Cornish *et al* 1998, Hwang *et al* 1997). When injecting a current into the sample via the electrodes electrode polarization, accumulated charge on the electrodes, and the counter-ions near the sample surface can introduce significant measurement errors (Gabriel *et al* 1996b, McAdams and Jossinet 1995, Rush *et al* 1960, Schwan and Kay 1956). The impedance of the skin can also contribute to the measurement errors (Lawler *et al* 1960, Ultchin *et al* 2002).

Magnetic induction spectroscopy (MIS) methods have been introduced for bio-impedance measurements in order to remove the need for electrodes to be in contact with the tissue or sample (Barai *et al* 2012, Gencer *et al* 2000, Hart *et al* 1998, Guardo *et al* 1995, Guardo *et al* 1997, Hutten *et al* 1998, Netz *et al* 1993, Richer *et al* 2005, Scharfetter *et al* 1999, Scharfetter *et al* 2002, Tarjan *et al* 1968). Instead of using electrodes for the injection of electrical current into tissue, MIS uses coils to produce magnetic fields that will induce currents within the tissue or sample. These induced currents also produce magnetic field perturbations that can be detected by sensor coils. The magnetic inductive methods thus overcome the challenges of the measurement errors resulting from electrodes in EIS. A further advantage of MIS is the removal of electrical hazards if equipment can cause large currents to flow through electrode contacts.

There have been a few types of MIS measurement systems developed by other research groups usually at the higher frequency end of the β dispersion range (Barai *et al* 2012, Hart *et al* 1998, Guardo *et al* 1995, Hutten *et al* 1998, Netz *et al* 1993, Richer *et al* 2005, Scharfetter *et al* 1999). Much of the development has been made by researchers developing magnetic induction tomography (MIT) systems to attempt to image the distribution of tissue conductivity within body segments (Griffiths *et al* 1999, Griffiths 2001, Korjenevsky and Cherepenin 1997, Korjenevsky *et al* 2000, Merwa *et al* 2004, Rosell *et al* 2001, Rosell-Ferrer *et al* 2006, Scharfetter *et al* 2001, Scharfetter *et al* 2002, Scharfetter *et al* 2005, Vauhkonen *et al* 2008, Watson *et al* 2003, Watson *et al* 2004, Watson *et al* 2008).

In this study, we developed a prototype magnetic induction spectroscopy gradiometer probe for bio-impedance measurements of cervical tissue over the frequency range of 50 kHz to 300 kHz. The objective of this work was to design a probe that could be used to make *in-vivo* measurements without the need for electrode contact with the tissue. The background to this objective was previous work showing that impedance spectroscopy is able to show changes in cervical tissue during pregnancy and to detect pre-malignant changes in cervical tissue (Abdul *et al* 2006 and Ghandi *et al* 2006).

The major requirement for measuring cervical tissue *in-vivo* using the MIS technique is that the measuring sensitivity is concentrated in the cervix with the minimization of induced signals from the surrounding tissues. The average size of human cervix is 2-3 cm in length and 2.5 cm in diameter (Kurman 1994). We have thus constructed a coaxial gradiometer probe with a magnetic concentrator made of ferrite rod and a magnetic confinement shield made of a ferrite cylinder. The diameter of the probe is 3 cm in order to measure the whole cervix and also to be compatible with the size of clinical spatula. The use of soft magnetic material, *i.e.* ferrite, has been widely applied in MIT systems for magnetic screening (Yu 1993, Peyton 1995, Peyton 1996, Peyton 1999). Unlike the MIT system with a large outer magnetic confinement surrounding all the coils, we have combined both magnetic concentrator and confinement shield on a single coaxial probe with the use of the gradiometer coils in order to optimize the signal sensitivity. The magnetic screening efficiency have been assessed both experimentally and computationally and compared with an air-cored gradiometer probe without magnetic screening. We have also simulated the induced current density in a disk larger than the cervix in order to investigate the signals from the surrounding tissue.

1.2 Theory

In MIS gradiometer systems, two sensing coils are placed at equal distances from the excitation coil and the sample is placed in front of one of the sensing coils. An alternating electric current flows through the excitation coil and generates the primary magnetic field. The magnetic field thus induces an electric field in the sample which generates electric eddy currents. The eddy currents in the sample then produce the secondary magnetic field. Both the primary and secondary magnetic fields produce an electromotive force (e.m.f.) in the sensing coils. When two sensing coils are connected together in anti-phase, the voltages induced by the primary magnetic field are cancelled out and only the difference from the secondary magnetic field remains. When the sample is placed nearby one of the sensing coils, whilst further away from the other, the e.m.f. in the two sensing coils are different due to the different distances to the sample. A quasi-static approximation of the e.m.f. can be given by

$$\frac{\Delta V}{V} = Pf\mu_0(2\pi f\varepsilon_0\varepsilon_r - j\sigma) + +Q\chi \qquad (1)$$

where ΔV is the e.m.f. from the secondary magnetic field, V is the e.m.f. from the primary magnetic field, μ_0 is the permeability in a vacuum, f is the frequency of the drive current, ε_0 is the permittivity in a vacuum, ε_r is the relative permittivity of the sample, σ is the electric conductivity of the sample, χ is the magnetic susceptibility of the sample, P and Q are geometrical factors related to sample size, shape and the distance from the coils (Griffiths 2005, Barai *et al* 2012).

The eddy currents in the sample generate both in-phase and quadrature signals ΔV in the sensing coils, compared with the primary signal V, which are given as the real and imaginary parts in equation (1), respectively. The out-of-phase signal of ΔV results from the resistive component of the sample and is proportional to the sample conductivity and drive frequency.

2. Method

2.1 Coil System

The ferrite-cored MIS gradiometer consists of an excitation coil and two sensing coils wound coaxially on a borosilicate glass former. A ferrite rod was inserted in the glass former as a magnetic concentrator and an outer cylindrical ferrite tube was used as a magnetic confinement shield. The end faces of the ferrite cylinder were open. An alternating source is connected to the excitation coil and the primary magnetic field is generated in proportion to the applied current. 30 turns of 0.4 mm enamelled copper wire (ecw) were used on the excitation coil and 40 turns of 0.1 mm ecw on the sensing coils and were all wound on a glass former of 15.0 mm in outer diameter. The spacing between each sensing coil and the excitation coil was 0.5 mm. A commercially available ferrite rod with diameter of 9.8 mm was placed inside the glass former and both were placed within a ferrite cylinder of 26.0 mm diameter.

An air-cored gradiometer with similar diameter was also constructed in comparison with the ferrite-cored probe. 60 turns of 0.2mm ecw were used on the excitation coil and 40 turns of 0.1 mm ecw on the sensing coils and they were wound tightly on a glass tube with an outer diameter of 30.0 mm and inner diameter of 26.0 mm. The spacing between each sensing coil and the excitation coil was 0.5 mm. Both gradiometers were made the same length (22.0 mm) as shown in figure 1.

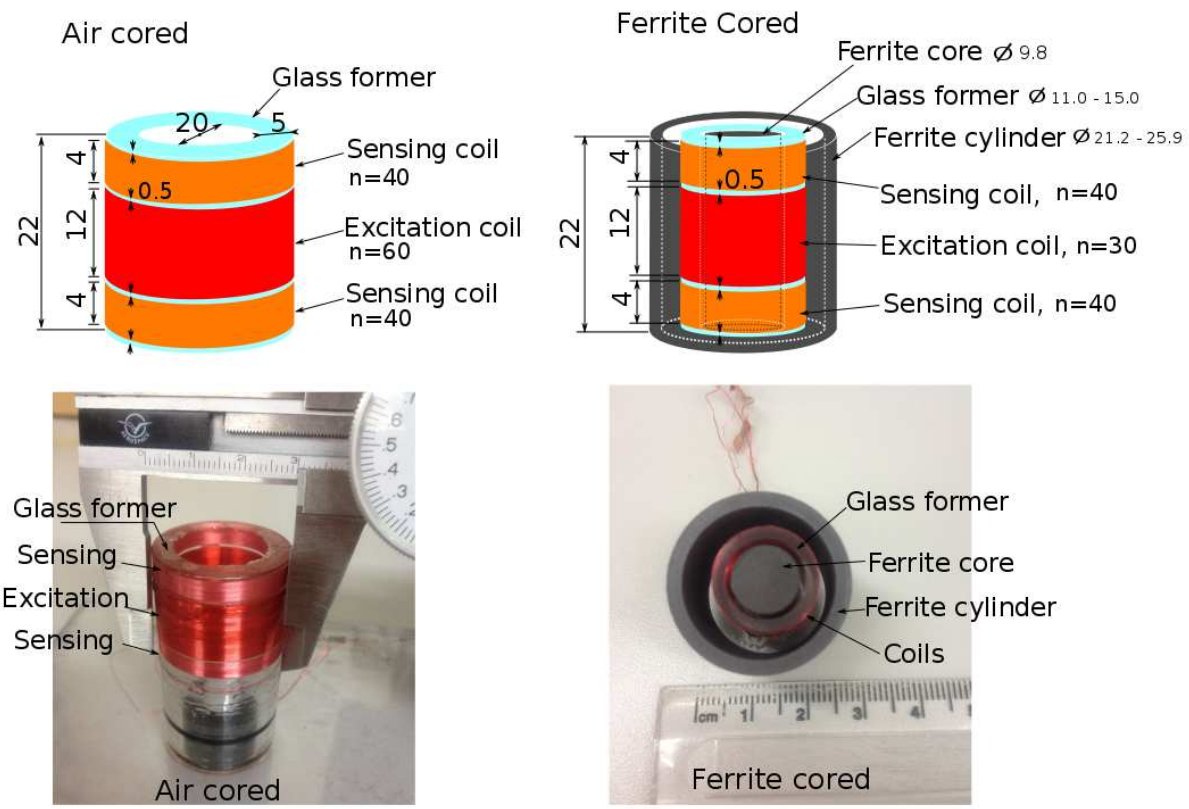

Figure 1 Air-cored and ferrite-cored coil systems with the lengths and diameters given in mm. Both ends of each probe were open.

2.2 Hardware

The drive coil was connected to a power amplifier whose input signal was controlled by a PC via a digital-to-analog interface (NI DAQ 6366, National Instruments). The drive and receive signals were controlled and processed by a computer program (NI LabView 2012) installed on the PC and interfaced with a digital-to-analog converter (NI-USB 6366). The drive signal operated at a sample rate of 2 M sample s^{-1} and with a DAQ resolution of 16 bits. Three excitation frequencies, 50 kHz, 100 kHz, and 300 kHz, were controlled by the PC, with an output amplitude of 20.0 V_{pp} and resulting drive currents of 0.57 A, 0.29 A, and 0.10 A, respectively. The PC controller used commercial software (LabView 2012, National Instruments). The receiver signal from the sensing coils was connected to a differential amplifier where any unbalanced signal was subtracted in order to optimize the signal from the sample. The block diagram of the MIS gradiometer system is shown in figure 2.

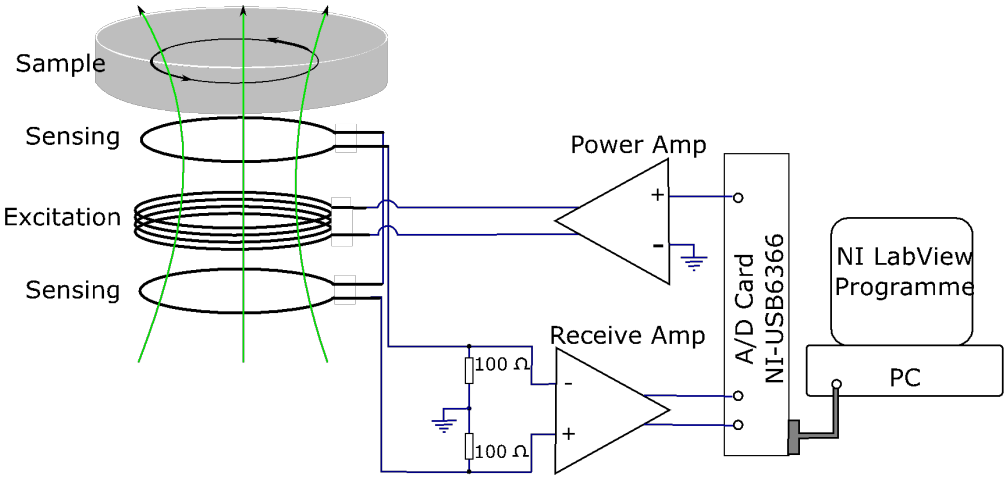

Figure 2 The block diagram of the MIS system. The differential receive amplifier was connected to two 100 Ω resistors, and thus the (output) signal sensitivity was not directly proportional to frequency.

2.3 Electric-field shielding

To induce the magnetic fields, relatively large drive voltages are required which may be of the order of 10^6 greater than detected signal. The MIT system is required to be sensitive only to perturbations in the magnetic field and insensitive to perturbations in the electric field and hence electric field shielding is required. Unlike normal shielding this shielding must be almost transparent to AC magnetic fields. For the air cored system, it was found that effective screening could be achieved with two layers of carbon-loaded conductive polyethylene (PE) film (electrical conductivity 125-127 S/m, thickness 75 μm, Black Conductive ESD-Safe Bag, RS Components Ltd., UK).

For the ferrite-cored *in-vivo* system there was not sufficient physical space for the PE film and hence a system based on a much thinner (about 10 μm) aluminum metalized polyethylene terephthalate (PET), with a surface resistivity of about 1 Ω·m, film was developed. In MIT systems, metal films cut in radial patterns were often used and recommended in order to prevent eddy current induced within the screening material itself (Peyton 1995, Korjenevsky 2000, Watson 2002, Peyton 2002, Goss 2003, Griffiths 2005). In this work, two layers of thin aluminum metalized PET films were used for the electric field shielding. On the probe face, the film was patterned in petals as shown in figure 3(a). An additional layer of conductive PE film was used to cover the sides and a gap was left to prevent eddy currents in each layer, as illustrated in the schematic figure (Figure 3b). This additional conductive PE layer was only added in order to make good contact with the earth ground wire.

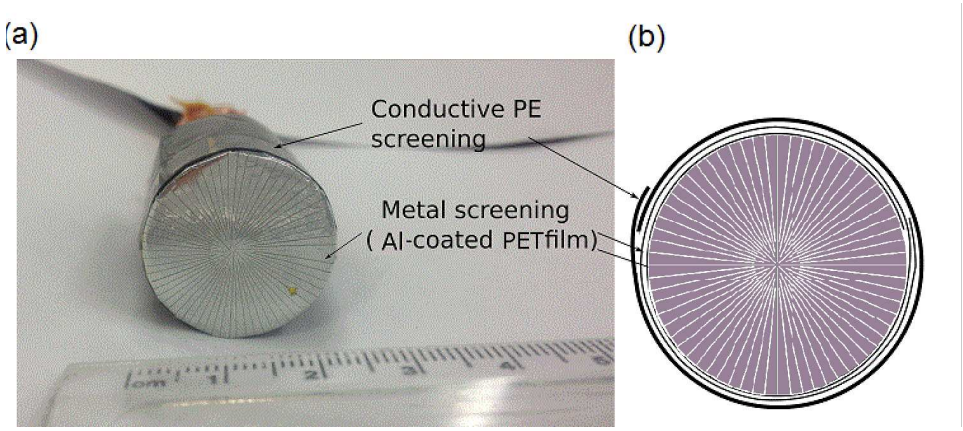

Figure 3 (a) The patterned electric-field screening for the MIS system. (b) The illustrated figure from the probe face: a PET-coated Al film was patterned on the probe face while a separate film was wrapped around the probe sides. A conductive PE film was covered on the Al film on the side of the probe.

2.4 Finite Element Method Simulations

Simulation using the Finite Element Method (FEM) was implemented using commercially available software (4.3b COMSOL Multiphysics). The aim of the simulation in this work was to design a ferrite-cored MIS probe with high magnetic screening efficiency and geometry compatible to the human cervix and vagina. The simulation model was adapted from a model, 'Mutual Inductance and Induced Currents in Multi-turn Coil', which can be obtained in COMSOL application library (COMSOL application). The built-in 'Magnetic Fields' physics mode within AC/DC Module from COMSOL Multiphysics was used where Maxwell's equations were solved numerically using the FEM analysis. The '2D Axisymmetric' geometric mode was chosen and simulated in cylindrical coordinates due to the coil and cervix geometry being axial-symmetric. Fine triangular meshes with the size between 0.5 – 0.001 mm were chosen for the FEM domains and the mesh distribution were automatically adopted to the geometry chosen by the software. The dimensions and geometries of the probe including the coils and ferrites were described in figure 1. The electrical conductivity and magnetic permeability of ferrites were set as 0 and 2000, respectively. An AC current source (0.3A peak) was set to drive the close-loop excitation coil with drive frequency 100 kHz

which is similar to our drive signal, and the induced voltages from both open-loop sensing coils were simulated. The induced current density in the sample versus the depth was also simulated for both air-cored and ferrite-cored gradiometer.

3. Measurements

3.1 Measurements with saline solutions

Conductivity measurements at the three frequencies (50 kHz, 100 kHz, and 300 kHz) were made using samples consisting of distilled water and four sodium chloride solutions, with conductivities within the range of 0.01-1.3 Sm^{-1}. The conductivities of distilled water and saline samples were measured using a commercial conductivity meter (Model 470, Spectronic analytical Instruments, UK). The samples were placed in a 0.6 L round plastic container and placed on top of each MIS gradiometer. The base of the plastic container was of thickness 2 mm. All measurements were performed at room temperature of 20.0 - 22.0 °C, with a variance of less than 1.0 °C during each measurement. Measurements were taken ten times for each sample. The effectiveness of the electric-field screening was determined by measuring the offset resulting from the measurements made on the distilled water and the saline solutions.

3.2 Magnetic shielding for surrounding

The objective was to construct gradiometers that would be sensitive to tissue placed in front of the transducer but insensitive to any surrounding tissue. This is particularly important for the proposed in-vivo measurements within the vagina. To determine the magnetic screening effectiveness, both air- and ferrite-cored MIS gradiometers were inserted into a cylindrical container with an inner hollow tube which had an outer diameter of 37.0 mm. The plastic container, with inner diameter of 60.0 mm, was filled with 1.1 Sm^{-1} saline and conductivity measurements were taken at a frequency of 100 kHz and at room temperature. Measurements were made by filling the cylinder with different depths of saline (l_c, from 5.0 mm below the probe face filled up to 36.0 mm) as shown in figure 4.

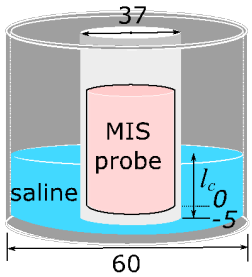

Figure 4 A cylindrical container was used to test the effectiveness of the magnetic screening.

3.3 Sensitivity measurements versus sample distance

A 1.02 Sm^{-1} saline sample was placed in a 0.6 L plastic round container with 12.0 cm inner diameter and 5 cm height. Measurements were taken by increasing the distance between the sample and the probe from 2.5 mm to 12.0 mm for the ferrite-cored probe. At each distance measurements were repeated 10 times and all the measurements were taken at room temperature with the drive frequency 100 kHz.

3.4 In-vivo measurements on human forearm and hand

In-vivo conductivity measurements were also performed on a human forearm using air-cored probe, and a human hand using ferrite-cored probe, at frequencies of 50 kHz, 100 kHz, and 300 kHz. A spacing of 2.5 mm was left between both MIS gradiometers and the forearm. Measurements were taken ten times for each frequency and each measurement was taken for ten seconds.

4. Results

4.1 Measurements with saline solutions

4.1.1 Conductivity measurements and signal sensitivity

Conductivity measurements on distilled water and four saline solutions were made with the air-cored and ferrite-cored MIS gradiometers at frequencies of 50 kHz, 100 kHz, and 300 kHz as described in section 3.1. Ten measurements were taken for each sample at each frequency. Figures 5(a) and (b) show the results using air-cored and ferrite-cored MIS gradiometers, respectively. The gradiometer output signals are plotted against the conductivity of the samples and a straight line was fitted to each drive frequency with five data points in each case. Signal sensitivity, defined as the slope of the fitted straight line, varies with frequency. The gradiometer output signals were amplified through a differential amplifier which was connected to two 100 Ω resistors as shown in figure 2 (to Receive Amp), and thus the sensitivity varied and was not proportional to the frequency predicted in theory.

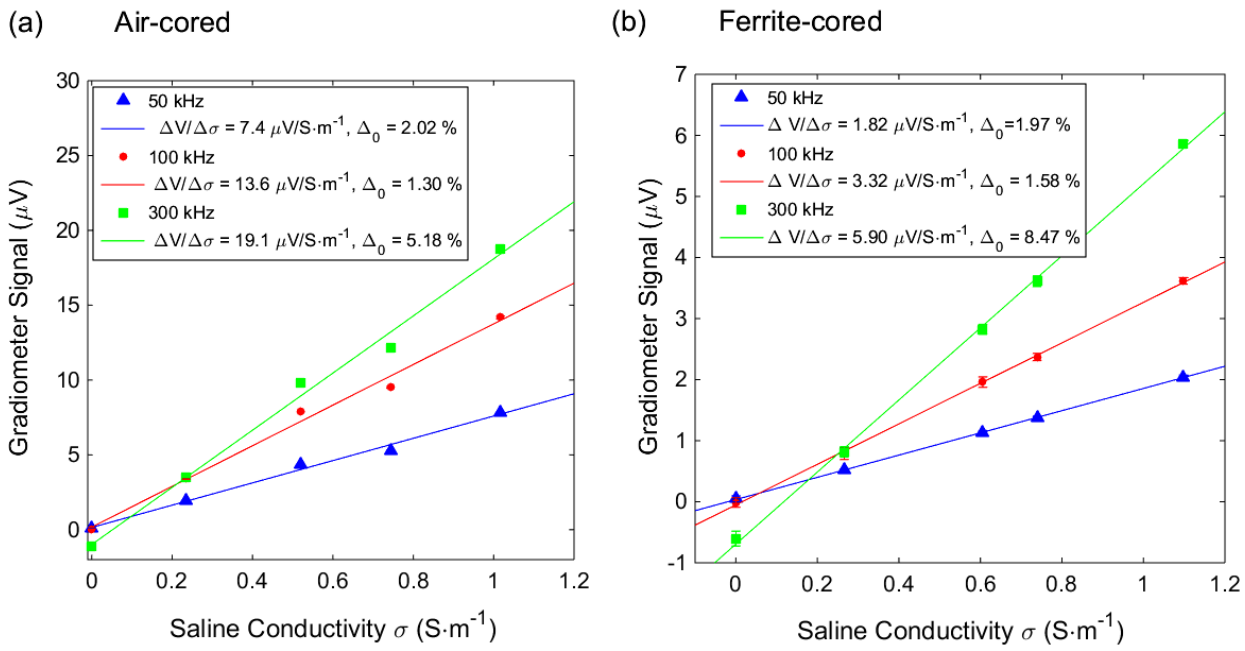

Figure 5 Results from the conductivity measurements using distilled water and four saline samples at frequencies 50 kHz, 100 kHz, and 300 kHz. (a) is the results from the air-cored probe and (b) is from ferrite-cored probe. A straight line is fitted to each data set with the slope as sensitivity S (=$\Delta V/\Delta\sigma$) and Δ_0 as the corresponding offset. Error bars represent the standard deviation from ten measurements.

4.1.2 Electric-field shielding

In this study, the effectiveness of the electric-field screening was determined by measuring the offset resulting from the measurements made on the distilled water and the saline solutions. In both figure 5(a) and 5(b), the E-field shielding efficiency was as high as 97% for lower frequencies 50 and 100 kHz with the offset less than 3% corresponding to the saline sensitivity, and 91% efficiency for 300 kHz with the corresponding offset less than 8.5%.

4.1.3 Characterization of system stability

The characterization of the system stability was also made by monitoring the output gradiometer signals without any sample at room temperature (with less than 1.0 °C variance) for at least 10 minutes, which was a much longer period of time compared to the sample measurements performed each time within 1 minute. The system stability corresponding to the measurement accuracy of the air-cored MIS probe was 0.09 Sm^{-1} at 50kHz, improving to 0.05 Sm^{-1} at 300 kHz. For the ferrite-cored MIS probe, the same corresponding measurement accuracy was 0.28 Sm^{-1} at 50 kHz, improving to 0.04 Sm^{-1} at 300 kHz.

4.2 Magnetic shielding for surroundings

4.2.1 Measurements from air-cored and ferrite-cored probe

The two MIS gradiometer types were inserted into a 1.02 Sm^{-1} saline cylinder filled to increasing depths. The gradiometer signals, normalized by the signal from a 0.6 L saline pot placed in front of the probe with spacing of 2.5 mm, were plotted against the depth of the saline at a frequency of 100 kHz as shown in figure 6. It can be seen that the maximum sensitivity to surrounding saline occurs when the saline surrounds half of the gradiometer (at 11.0 mm). It can also be seen that the ferrite-cored gradiometer is less sensitive than the air cored gradiometer to the surrounding saline. The maximum contribution from the surrounding saline, i.e. when the saline was filled up to half length of the probe, were also compared with the simulation results as shown in table 1. The combination of a ferrite core and ferrite screen has the highest magnetic shielding effectiveness compared with either the air cored or unscreened ferrite probes.

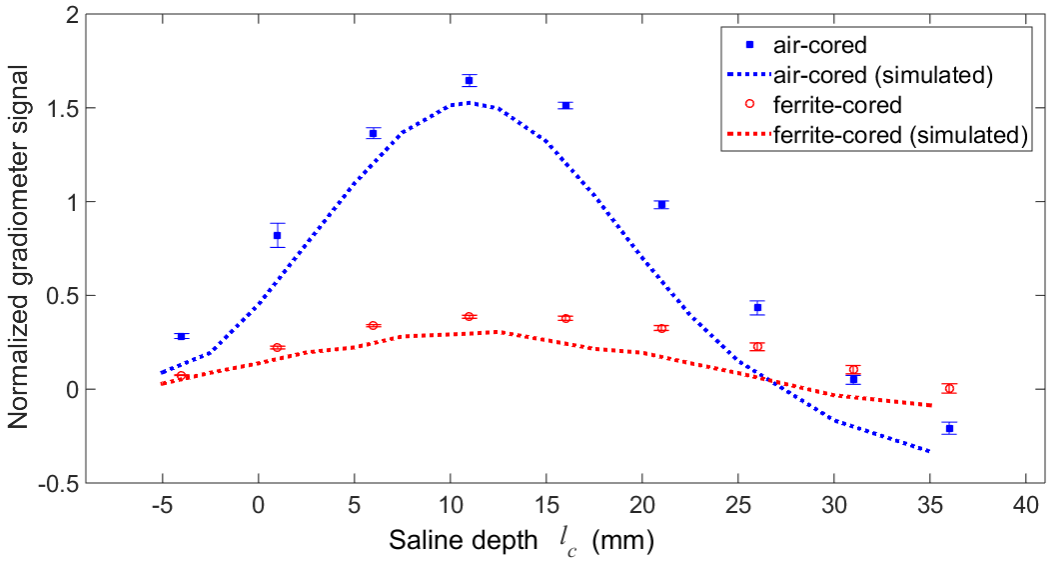

Figure 6 Results from magnetic shielding for surrounding tissues at drive frequency 100 kHz. 1.02 Sm^{-1} saline was filled to different depths of the cylinder which surrounded the MIS probes. Error bars represent the standard deviation from ten measurements.

Table 1. Maximum contribution from surrounding tissues to the normalized gradiometer signal. Gradiometer signal was normalized by the signal of a 0.6 L saline pot placed in front of the probe with spacing of 2.5 mm.

Probe Type	Air Cored		Ferrite Cored		Ferrite Core Only	Ferrite Screen Only
	measured	simulated	measured	simulated	simulated	simulated
Normalized gradiometer signal	1.65	1.52	0.38	0.31	1.08	0.45

4.2.2 Simulations

Simulation used the Finite Element Method (FEM) was implemented using commercially available software (4.3b COMSOL Multiphysics). Both the induced current in the sample and the gradiometer sensitivity were simulated for both types of MIS gradiometer. 2D and 3D axial-symmetric simulation results of magnetic flux density and induced current density were plotted in cylindrical coordinates as shown in figure 7. In figure 7(a) air-cored probe and (b) ferrite-cored probe, the 2D magnetic flux density is plotted in cylindrical coordinates and taken from a cross-sectional area (r versus z axis) from $r=0$ to $r=40$ *mm* with the rotational axis at $r=0$. Small distributed arrows represent the directions of the magnetic flux. The magnetic field was confined by the geometry of the ferrites for the ferrite-cored system in figure 7(b), unlike the air-cored system where the coils are surrounded by magnetic flux. The 2D induced current density in saline samples simulated for both coil systems are shown in figure 7(c) and (d). For the air-cored

system in figure 7(c), the induced current density is higher in the surrounding saline than in the saline near the probe face where the saline is further away from the drive coil. For the ferrite-cored system in figure 7(d), the induced current density distributes near the probe face similar to the coil radius and is confined by the probe geometry. The '3D' induced current density in the saline sample for air-cored (e) and for ferrite-cored (f) are taken as the rotational axisymmetric profile from figure 7(c) and (d) and plotted as volumetric figures, i.e. to rotate the 2D profile along z-axis cylindrically to form a 3D figure.

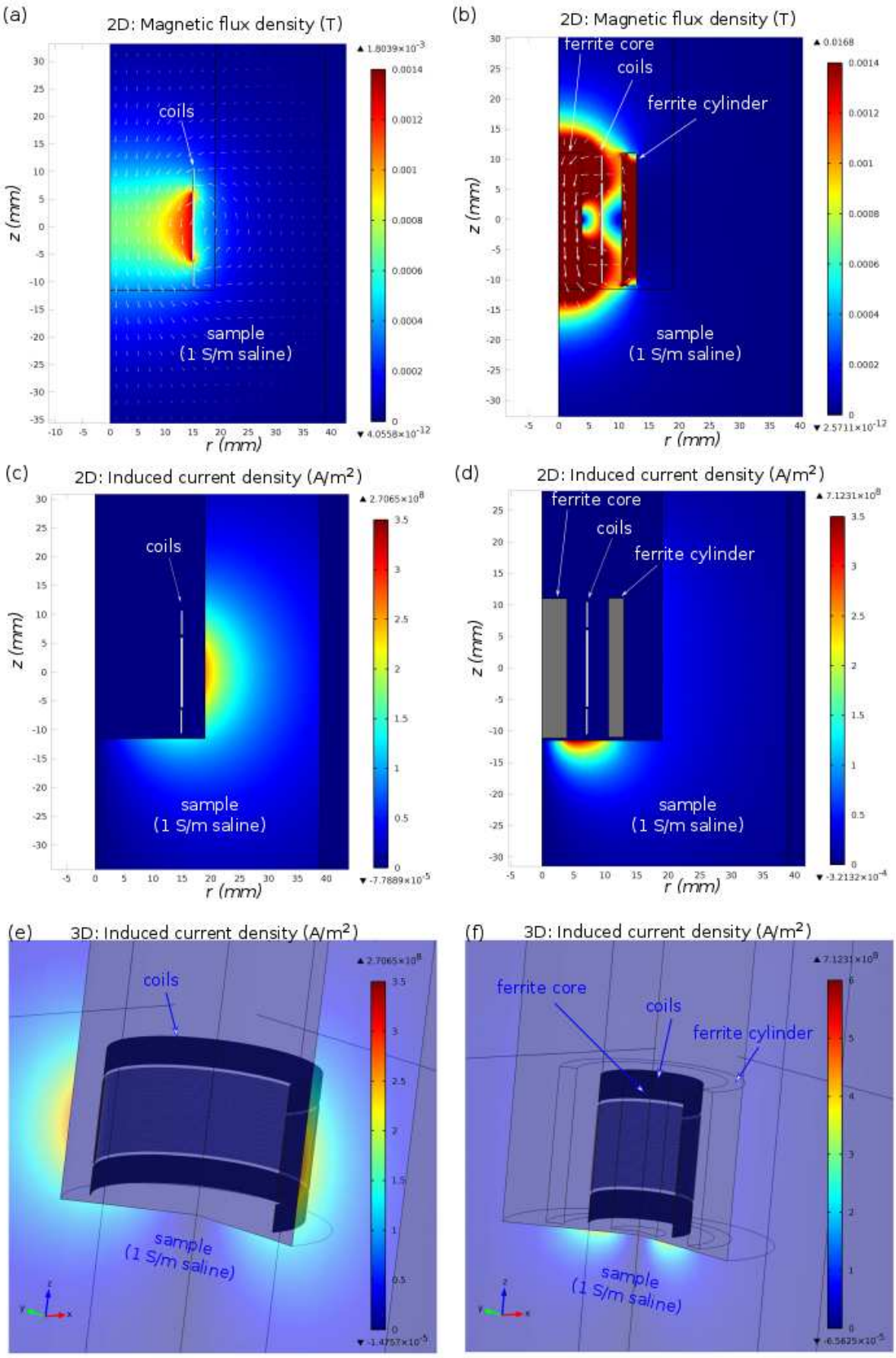

Figure 7 Simulation results from both air-cored and ferrite-cored MIS gradiometers. The axial-symmetric 2D magnetic flux density for the air-cored system shown in (a) and for the ferrite-cored system shown in (b). Small distributed arrows represent the directions of the magnetic flux. The 2D induced current density in saline samples simulated for both coil systems is shown in (c) air-cored and (d) ferrite-cored. The '3D' induced current density in the saline sample for air-cored probe in (e) and for the ferrite-cored probe in (f) are taken as the axial-rotational profiles from (c) and (d). The maximum induced current densities as

shown above each color scale bar are the induced current in the coils, while the values below the color scale bars are the minimum induced current density in this case, which appeared to be non-zero due to iteration limitations.

4.4 Sensitivity versus sample distance and signal penetration depth

4.4.1 Sensitivity measurements versus sample distance

Conductivity measurements were performed on a 0.6 L and 1.02 $S \cdot m^{-1}$ saline sample (12.0 cm diameter and 5.0 cm in height) with various spacings between the ferrite-cored probe and the sample. The gradiometer signal related to the sample conductivity was normalized by the signal when the sample was placed at a distance of 2.5 mm. The measurements were taken with a spacing of 2.5 mm up to 12.0 mm for the ferrite-cored probe as shown in figure 8. FEM simulated results using COMSOL was also plotted in figure 8. The measured results were similar to the simulated results.

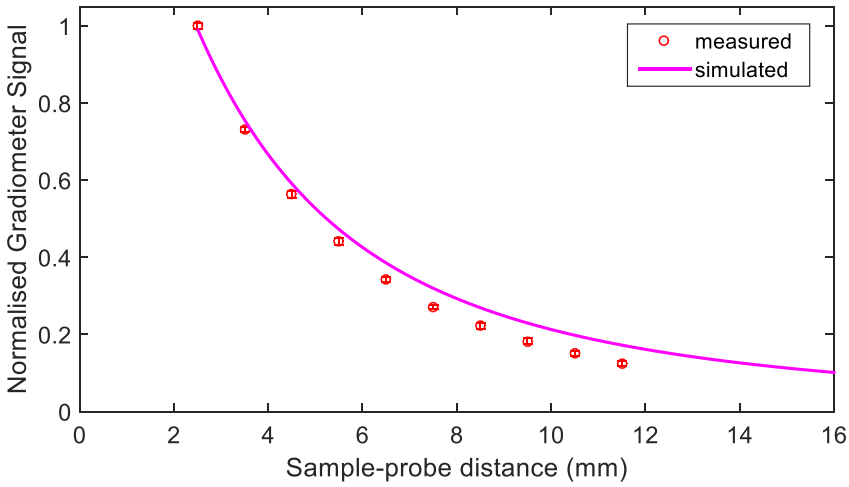

Figure 8 Results from sensitivity measurements and simulations against sample distance. The gradiometer signal was normalized by the signal when the sample was placed at a distance of 2.5 mm.

4.4.2 Signal penetration versus sample depth simulation

The simulated induced current density (phi component, J_{phi}) in the sample was plotted both longitudinally and radially as shown in figure 9 which provided the information of the 'signal penetration depth' into the sample. In figure 9(a), normalized J_{phi} from both air-cored and ferrite-cored probe were plotted against z-coordinate, with the probe face at z = -11 mm as shown in figure 7(c) and 7(d). Both curves were normalized with the maximum J_{phi}, where the maximum J_{phi} value was at r = 15 mm for air-cored probe and at around r = 6 mm for ferrite-cored probe within the sample. For the ferrite-cored probe, J_{phi} falls off rapidly and was less than 5 % when z > 30 mm beyond the surface of the cervix. For the air-cored probe, the signal falls off less rapidly than the ferrite-cored probe as no magnetic concentrator was used. In figure 9(b), normalized J_{phi} from ferrite-cored probe at z = -11.5, -13.5, and -15.5 mm was plotted against r. A fitted power curve ($y=a \cdot x^{-2}+b$) to z=-11.5 mm was plotted in the inset which shows the induced current density falls off as $1/r^2$ when r is larger than 15 mm, *i.e.* the radius of cervix.

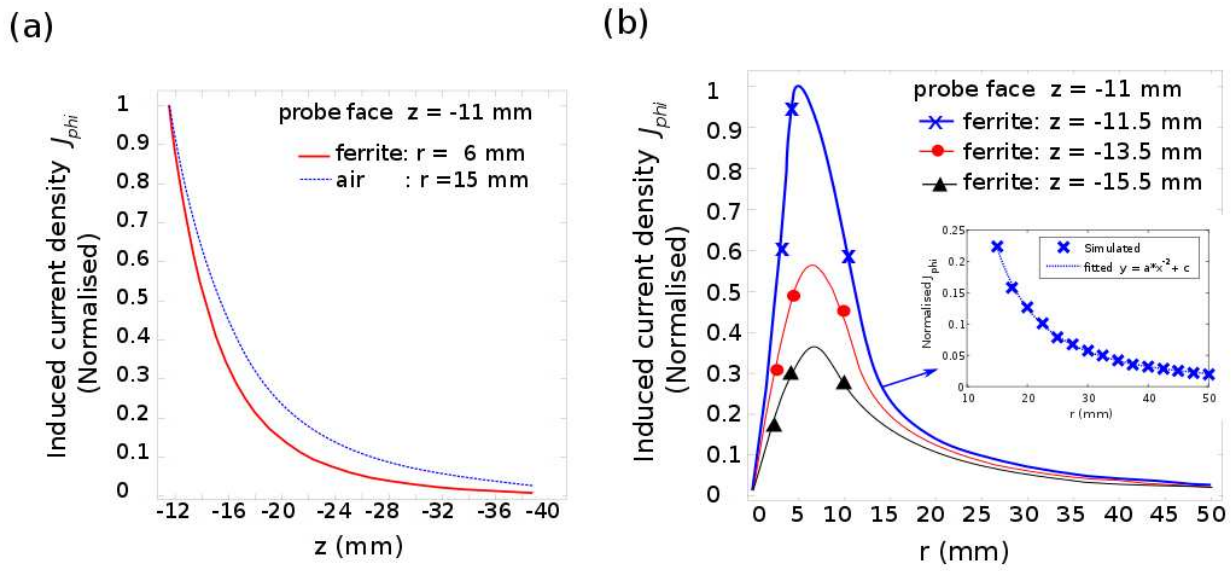

Figure 9 Simulation results of normalized induced current density J_{phi} within a 1.0 S·m^{-1} saline sample. (a) Normalized J_{phi} from both air-cored and ferrite-cored probe was plotted against z. (b) Normalized J_{phi} from the ferrite-cored probe was plotted against r, and the inset shows a fitted curve to results at z = -11.5 mm where J_{phi} falls off in the rate of $1/r^2$.

4.5 Impedance measurements on human forearm and hand

In-vivo impedance measurements were performed on a human forearm using the air cored probe and on a human hand using ferrite probe, at three frequencies 50 kHz, 100 kHz, and 300 kHz. Measurements were repeated 10 times for each frequency. The results are plotted as electrical resistivity, *i.e.* the inverse of conductivity, versus frequency as shown in figure 10. The results were presented in resistivity rather than conductivity, in order for both future reference and previous work on cervical tissue measurements (Ghandi 2006). These results are similar to the measured conductivities (2.6±0.4) reported by Chumlea *et al* (Chumlea 1988) using four-electrode method with drive frequency at 50 kHz.

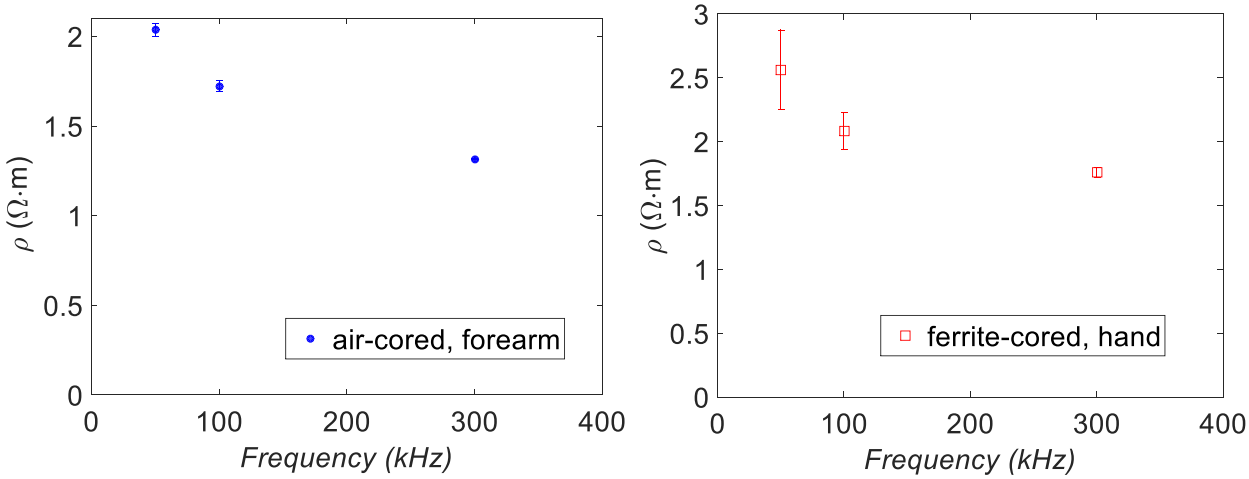

Figure 10 Results from measurements of the electrical resistivity (ρ) of in vivo tissue when a human forearm and hand were placing on the face of the air cored and ferrite-cored probes, respectively. Measurements were made at three frequencies (50 kHz, 100 kHz, and 300 kHz). Error bars represent the standard deviation from ten measurements.

5. Discussion

The design of a ferrite-cored magnetic induction probe with the use of a ferrite rod and ferrite tube confined the field largely to the volume within and in front of the gap between the ferrite core and the outer cylinder. This significantly screened out the signals from surrounding tissues, which made the measurement of cervical tissue practical. An air-cored probe without any magnetic screening was also constructed and tested, and the signal from the surrounding tissue was larger than the signal from cervical tissue.

Experimental measurements made using saline containers placed on the gradiometers showed similar sensitivities for both air and ferrite-cored probe. In both cases, sensitivity increased with frequency as was expected from the theoretical analysis. The sensitivity was expected on theoretical grounds to increase as the square of frequency for a constant current drive, but to fall linearly with frequency when using constant voltage drive. Figure 10 shows that sensitivity does increase with frequency between 50kHz and 100 kHz but somewhat less between 100kHz and 300kHz. This is due to the Thévenin output impedance (about 1 Ω) of the power amplifier.

The measurements made on the arm and hand show slightly different results between the two probes. The air-cored probe is sensitive to tissues at a greater depth than the ferrite-cored design as shown in simulation results of the induced current density versus sample depth. This might explain the fall in resistivity with frequency when using the air cored gradiometer as muscle tissue will have been within the sensitive volume, while skin tissue with higher resistivity will mainly be within the sensitive volume for ferrite-cored gradiometer. Muscle tissue has a lower dispersion frequency than the more superficial tissues. The results from the ferrite-cored gradiometer on a human hand has also shown a larger variance from ten repeated measurements, which could be the result of the intrinsic geometry of the tissue surface not making full contact with the probe face. It has also indicated the higher sensitivity of the ferrite-cored gradiometer towards the sample surface. However, more extensive measurements are needed before a firm conclusion can be drawn.

From the simulated results, the induced current density J_{phi} falls off rapidly longitudinally and contributes less than 5% of the normalised signal when beyond the surface of the cervix. In the radial direction, the induced current density J_{phi} falls off with the speed of $1/r^2$ from our simulation and fitted curve. To eliminate the signals from tissues surrounding the cervix, though not included in this work, the outer ferrite screening tube could be replaced with a longer geometry in future improvements of the probe.

The results shown that a ferrite-cored gradiometer design incorporating an air gap between the core and outer cylinder of ferrite does provide significantly reduced sensitivity to surrounding tissues as opposed to the sensitivity to tissues placed directly in front of the face of the probe. However, whilst the ferrite-cored probe has been shown able to make in-vivo measurements there is still scope for improvements, particularly in the thermal stability.

Acknowledgement: We thank Dr Tim Good for his technical advice and input. This work was funded by National Institute for Health Research (NIHR Ref Number II-ES-0511-21004).
Ethics: The Yorkshire and Humber National Research Ethics Committee granted approval for the relevant aspects of this work (Ref Number 13/YH/0167)

References

Abdul S, Brown B H, Milnes P and Tidy J A 2006 The use of electrical impedance spectroscopy in the detection of cervical intraepithelial neoplasia *International Journal of Gynecological Cancer* ***16*****(5)** 1823-32

Aberg P, Nicander I, Hansson J, Geladi P, Holmgren U and Ollmar S 2004 Skin cancer identification using multifrequency electrical impedance-a potential screening tool *Biomedical Engineering, IEEE Transactions on* **51(12)** 2097-2102

Barai A, Watson S, Griffiths H and Patz R 2012 Magnetic induction spectroscopy: non-contact measurement of the electrical conductivity spectra of biological samples *Meas. Sci. Technol.* **23** 085501

Burger H C and van Dongen R 1960 Specific electric resistance of body tissues *Phys. Med. Biol.* **5** 431-47

Chumlea W C, Baumgartner R N and Roche A F 1988 Specific resistivity used to estimate fat-free mass from segmental body measures of bioelectric impedance *The American Journal of Clinical Nutrition* **48(1)** 7-15

Cornish B H, Thomas B J and Ward L C 1998 Effect of temperature and sweating on bioimpedance measurements *Applied Radiation and Isotopes* **49(5)** 475-76.

COMSOL Application 12687 Mutual Inductance and Induced Current Density in Multi-Turn Coil *https://www.comsol.com/model/download/313891/models.acdc.mutual_inductance_multiturn.pdf*

Dean D A, Ramanathan T, Machado D and Sundararajan R 2008 Electrical impedance spectroscopy study of biological tissues *Journal of electrostatics* **66(3)** 165-77

Foster K R and Schwan H P 1995 Dielectric properties of tissues *Handbook of biological effects of electromagnetic fields* **2** 25-102

Gabriel C, Gabriel S and Corhout E 1996a The dielectric properties of biological tissues: I. Literature survey *Phys. Med. Biol.* **41** 2231-49

Gabriel S, Lau R W and Gabriel C 1996b The dielectric properties of biological tissues: II Measurements in the frequency range 10 Hz to 20 GHz *Phys. Med. Biol.* **41** 2251-69

Gandhi S V, Walker D, Milnes P, Mukherjee S, Brown B H and Anumba DO 2006 Electrical impedance spectroscopy of the cervix in non-pregnant and pregnant women *European Journal of Obstetrics & Gynecology and Reproductive Biology* **129(2)** 145-49

Gersing E 1998 Impedance spectroscopy on living tissue for determination of the state of organs. *Bioelectrochemistry and bioenergetics* **45(2)** 145-49

Gencer N G and Tek M N 2000. Imaging tissue conductivity via contactless measurements: a feasibility study. *Turkish Journal of Electrical Engineering & Computer Sciences* **6** 183-200.

Goss D, Mackin R O, Crescenzo E, Tapp H S and Peyton A J 2003 Understanding the coupling mechanisms in high frequency EMT *3rd World Congress on Industrial Process Tomography (Banff, Canada)* 364-69

Griffiths H, Stewart W R and Gough W 1999 Magnetic induction tomography: a measuring system for biological tissues *Ann. New York Acad. Sci.* **873** 335-45

Griffiths H 2001 Magnetic induction tomography *Meas. Sci. Technol.* **12** 1126

Griffiths H 2005 Magnetic Induction Tomography in *Electrical Impedance Tomography: Methods, History, and Applications* ed Holder D S *(Bristol: Institute of Physics Publishing)* 229-53

Guardo R, Trudelle S, Adler A, Boulay C and Savard P 1995 Contactless recording of cardiac related thoracic conductivity changes *Proc. IEEE 17th EMBS Conf.* **2** 1581-82

Guardo R, Charron G, Goussard Y and Savard P 1997 Contactless measurement of thoracic conductivity changes by magnetic induction *Proc. 19th EMBS Conf.* **6** 2450-53

Halter R J, Hartov A, Heaney J A, Paulsen K D and Schned A R 2007 Electrical impedance spectroscopy of the human prostate *IEEE Trans. Biomed. Eng.* **54** 1321-27

Hart F X and Dunfee W R 1993 In vivo measurement of the low-frequency dielectric spectra of frog skeletal muscle *Phys. Med. Biol.* **38** 1099-1112

Hart L W, Ko H W, Meyer J H, Vasholz D P and Joseph R I 1988 A noninvasive electromagnetic conductivity sensor for biomedical applications *Biomed. Engin. IEEE Trans.* **35** 1011-22.

Hutten H, Scharfetter H, Ninaus W, Puswald B, Petrova G I and Kovachev D 1998 Inductively coupled wideband transceiver for bioimpedance spectroscopy (IBIS) *Proc. IEEE 20th EMBS Conf.* **4** 1791-94

Hwang J H, Kirkpatrick K S, Mason T O and Garboczi E J 1997 Experimental limitations in impedance spectroscopy: Part IV Electrode contact effects *Solid State Ionics* **98(1)** 93-104

Lawler J C, Davis M J and Griffith E C 1960 Electrical characteristics of the skin *The Journal of Investigative Dermatology* **34** 301-8

Kerner T E, Paulsen K D, Hartov A, Soho S K and Poplack S P 2002 Electrical impedance spectroscopy of the breast: clinical imaging results in 26 subjects *IEEE Trans. Med. Imag.* ***21*****(6)** 638-645

Kraszewski A, Stuchky S S, Stuchly M A and Smith A M 1982 *In vivo* and *in vitro* dielectric properties on animal tissues at radio frequencies *Bioelectromagnetics* **3** 421-32

Korjenevsky A and Cherepenin V A 1997 Magnetic induction tomography. *J. Commun. Technol. Elec.* **42** 469-74

Korjenevsky A, Cherepenin V and Sapetsky S 2000 Magnetic induction tomography: experimental realization *Physiol. Meas.* **21** 89

Kurman, edited by Robert J 1994 *Blaustein's Pathology of the Female Genital Tract* (4th ed.) NY: Springer New York. 185–201

Martinsen O G and Grimnes S 2011 *Bioimpedance and bioelectricity basics*. Academic press. 179-253

McAdams E T and Jossinet J 1995 Tissue impedance: a historical overview *Physiol. Meas.* **16** A1-A13

Merwa R, Hollaus K, Biró O and Scharfetter H 2004 Detection of brain oedema using magnetic induction tomography: a feasibility study of the likely sensitivity and detectability *Physiol. Meas.* **25** 347

Miklavcic D, Pavselj N and Hart FX 2006 Electric properties of tissues *Wiley encyclopedia of biomedical engineering*

Netz J, Forner E and Haagemann S 1993 Contactless impedance measurement by magnetic induction-a possible method for investigation of brain impedance *Physiol. Meas.* **14** 463

Osterman KS 2004 Non-invasive assessment of radiation injury with electrical impedance spectroscopy. *Phys. Med. Biol.* **49** 665–83

Peyton A J 1995 Mutual inductance tomography *Process Tomography: Principles, Techniques, and Applications* 85-100

Peyton A J, Yu Z Z, Lyon G, Al-Zeibak S, Ferreira J, Velez J, Linhares F, Borges A R, Xiong H L, Saunders N H and Beck M S 1996 An overview of electromagnetic inductance tomography: description of three different systems *Meas. Sci. Technol.* **7** 261-271

Peyton A J, Beck M S, Borges A R, de Oliveria J E, Lyon G M, Yu Z Z, Brown M W and Ferreira J 1999 Development of electromagnetic tomography (EMT) for industrial applications. Part 1: sensor design and instrumentation *1st World Congress on Industrial Process Tomography, Buxton, Greater Manchester 1999* 306-312

Peyton A J, Watson S, Williams R J, Griffiths H and Gough W 2002 Characterising the effects of the external electromagnetic shield on a magnetic induction tomography sensor *3rd World Congress on Industrial Process Tomography, Banff, Canada 2002* 352-357

Richer A and Adler A 2005 Eddy current based flexible sensor for contactless measurement of breathing *IEEE Proc. Instrum. Meas. Techn. Conf. IMTC 2005* **1** 257-60

Rosell J, Casanas R and Scharfetter H 2001 Sensitivity maps and system requirements for magnetic induction tomography using a planar gradiometer *Physiol. Meas.* **22** 121

Rosell-Ferrer J, Merwa R, Brunner P and Scharfetter H 2006 A multifrequency magnetic induction tomography system using planar gradiometers: data collection and calibration *Physiol. Meas.* **27** S271.

Rush S, Abildskow J A and McFee R 1963 Resistivity of body tissues at low frequencies *Circ. Res.* **12** 40-50

Scharfetter H, Ninaus W, Puswald B, Petrova G I, Kovachev D and Hutten H 1999 Inductively Coupled Wideband Transceiver for Bioimpedance Spectroscopy (IBIS) *Ann. New York Acad. Sci.* **873** 322-34

Scharfetter H, Lackner H K and Rosell J 2001 Magnetic induction tomography: hardware for multi-frequency measurements in biological tissues *Physiol. Meas.* **22** 131

Scharfetter H, Riu P, Populo M and Rosell J 2002 Sensitivity maps for low-contrast perturbations within conducting background in magnetic induction tomography *Physiol. Meas.* **23** 195

Scharfetter H, Casañas R and Rosell G 2003 Biological tissue characterization by magnetic induction spectroscopy (MIS): requirements and limitations *IEEE Trans. Biomed. Eng.* **50** 870-80

Scharfetter H, Merwa R and Pilz K 2005 A new type of gradiometer for the receiving circuit of magnetic induction tomography (MIT) *Physiol. Meas.* **26** S307

Schwan H P and Kay F C 1956 Specific resistance of body tissues *Circ. Res.* **4** 664-670

Schwan H P and Kay C F 1957 The conductivity of living tissues *Ann. N. Y. Acad. Sci.* **65(6)** 1007-13

Schwan H P and Foster K R 1980 RF-field interactions with biological systems: Electrical properties and biophysical mechanisms *Proceedings of the IEEE* **68** 104-13

Schwan H P 1994 Electrical properties of tissues and cell suspensions: mechanisms and models *IEEE 16th EMBS Conf.* **1** A70-A71

Stoy R D, Foster K R and Schwan H P 1982 Dielectric properties of mammalian tissues from 0.1 to 100 MHz; a summary of recent data *Phys. Med. Biol.* **27(4)** 501

Tarjan P P and McFee R 1968 Electrodeless measurements of the effective resistivity of the human torso and head by magnetic induction *IEEE Trans. Biomed. Eng.* **4** 266-78

Ultchin Y, Nachaliel U and Ori A 2002 Indirect calculation of breast tissue impedance values *Physiol. Meas.* **23** 177-182

Vauhkonen M, Hamsch M and Igney C H 2008 A measurement system and image reconstruction in magnetic induction tomography *Physiol. Meas.* **29** S445

Watson S, Wiliams R J, Morris A, Gough W and Griffiths H 2002 The Cardiff magnetic induction tomography system *Proc. Int. Fed. Med. Biol. Eng. EMBEC92, Vienna Austria, Dec. 2002,* **3(1)**, 116-117

Watson S, Williams R J, Griffiths H, Gough W and Morris A 2003 Magnetic induction tomography: phase versus vector-voltmeter measurement techniques *Physiol. Meas.* **24** 555

Watson S, Morris A, Williams R J, Griffiths H and Gough W 2004 A primary field compensation scheme for planar array magnetic induction tomography *Physiol. Meas.* **25** 271

Watson S, Williams R J, Gough W and Griffiths H 2008 A magnetic induction tomography system for samples with conductivities below 10 S m^{-1} *Meas. Sci. Technol.* **19** 045501

Yamamoto Y and Yamamoto T 1987 Measurement of electrical bio-impedance and its applications *Medical progress through technology* Springer Netherlands 171-183

Yu Z Z, Peyton A T, Beck M S, Conway W F and Xu L A 1993 Imaging system based on electromagnetic tomography (EMT) *Electronics Letters* **29** 625-626